ORIGINAL RESEARCH PAPER
Volume - 14 | Issue - 05 | May - 2025 | PRINT ISSN No. 2277 - 8179 | DOI : 10.36106/ijsr
INTERNATIONAL JOURNAL OF SCIENTIFIC RESEARCH

TURMERIC-MEDIATED SYNTHESIS OF MANGANESE OXIDE NANOPARTICLES WITH POTENT ANTI-DENGUE, APOPTOSIS AND CYTOTOXIC ACTIVITIES

Chemical Science

Nagat Mohammad Ehmadi Barak Department Of Chemistry Sam Higginbottom University Of Agriculture Technology & Sciences, Allahabad 211007, Up India

Dr. Amit Chattree Department Of Chemistry Sam Higginbottom University Of Agriculture Technology & Sciences, Allahabad 211007, Up India

Dr. Shabnam. Dan Department Of Chemistry Sam Higginbottom University Of Agriculture Technology & Sciences, Allahabad 211007, Up India

ABSTRACT

Manganese oxide nanoparticles (MnO NPs) have emerged as promising candidates in biomedical applications due to their distinct physicochemical, redox-active, and catalytic properties, which are particularly advantageous in cancer therapeutics. The present study investigates the biological and biochemical properties of turmeric-mediated manganese oxide nanoparticles (MnNPs) specifically MN05 and MN11 focusing on their antibacterial, anti-dengue, and cytotoxic activities. Nanoparticles were synthesized via green methods and evaluated through a combination of molecular, enzymatic, and cellular assays. Reverse transcription PCR (RT-PCR) targeting the DENV-2 gene revealed a concentration-dependent suppression of viral gene expression, with significant downregulation observed at ≥375 µM, particularly for MN05. Gel electrophoresis confirmed reduced amplification in treated samples, indicating transcriptional suppression or viral RNA degradation. Flow cytometry analysis demonstrated corresponding shifts in cell morphology and complexity, with high-dose treatments leading to increased cell granularity and size, suggesting nanoparticle uptake and stress responses. MN05 showed a more gradual response pattern, while MN11 triggered more abrupt changes. In parallel, superoxide dismutase (SOD) activity assays highlighted the superior antioxidant potential of MN05, which consistently outperformed MN11 across all tested concentrations. The activity declined at higher doses, suggesting oxidative stress beyond a therapeutic threshold. Overall, the findings demonstrate that turmeric-derived MnNPs, especially MN05, exhibit potent antiviral, antioxidant, and cytotoxic properties, making them strong candidates for further exploration in nanomedicine-based dengue therapy and beyond.

KEYWORDS

Turmeric, Manganese oxide, green synthesis, apoptosis, DENV-2, DCFH-DA, SOD, ROS

1.1 INTRODUCTION

Nanotherapy has gained significant attention as a cutting-edge approach to overcoming the limitations of conventional melanoma treatments, particularly in terms of drug resistance, nonspecific targeting, and systemic toxicity. Among the various nanomaterials explored, manganese oxide nanoparticles (MnO NPs) have emerged as a promising class of therapeutic agents owing to their unique physicochemical properties, biocompatibility, and redox activity. MnO NPs can be strategically engineered to serve as efficient drug carriers, enabling enhanced bioavailability, tumor-targeted delivery, and controlled release of therapeutic agents. Their intrinsic ability to generate reactive oxygen species (ROS) and modulate the tumor microenvironment further enhances their anticancer efficacy. When applied to melanoma, MnO NPs exhibit strong potential to accumulate preferentially in tumor tissues, thereby increasing localized drug concentration while minimizing off-target effects. Moreover, the redox-responsive behavior of MnO NPs allows them to act synergistically with chemotherapeutic drugs, potentially overcoming multidrug resistance mechanisms and improving treatment outcomes. This dual function both as a drug delivery platform and as an active therapeutic agent positions MnO NPs at the forefront of nanomedicine-driven melanoma therapy.

Use of plant extract-mediated reduction methods represents a more sustainable and effective green approach for the synthesis of metal nanoparticles. Compared to microbial methods, plants offer distinct advantages due to the diverse range of bioactive molecules present in their extracts, which can function as both reducing and capping agents **(Duran et al., 2005; Duran et al., 2011; Narayanan, 2010).** This rich biochemical diversity enhances the rate of nanoparticle reduction and stabilization, allowing the synthesis process to be conducted under mild conditions, including lower reaction temperatures and atmospheric pressure **(Carmona, 2010).**

Manganese oxide nanoparticles (MnO NPs) have emerged as effective agents with broad-spectrum antibacterial activity, making them attractive for various biomedical applications. Their antibacterial mechanism is largely attributed to the generation of reactive oxygen species (ROS), which induce oxidative damage to bacterial membranes and intracellular components, ultimately leading to cell death **(Singh et al., 2018)**. The small particle size and high surface area of MnO NPs enhance their interaction with bacterial cells, improving their efficacy **(Jayandran et al., 2015).** Furthermore, MnO NPs can disrupt bacterial metabolism by interfering with enzymatic activity and cellular respiration, primarily due to their redox potential and surface reactivity **(Kumar et al., 2021).** Notably, MnO NPs have demonstrated antibacterial effects against both Gram-positive and Gram-negative bacteria, including E. coli and S. aureus **(Ramesh et al., 2020)**. The green synthesis approach particularly using plant extracts like turmeric has further enhanced their biological activity by introducing bioactive phytochemicals that act synergistically with the nanoparticles **(Barka et al., 2024).** These features not only underscore the therapeutic potential of MnO NPs but also highlight their relevance as sustainable alternatives to conventional antimicrobials in the face of growing antibiotic resistance.

Manganese oxide nanoparticles (MnO NPs) have recently gained attention for their promising antiviral properties, particularly in the context of dengue fever a rapidly spreading mosquito-borne viral disease that affects millions globally. With the lack of specific antiviral drugs and growing limitations in traditional mosquito control methods, there is a pressing need for alternative therapeutic and preventive strategies **(Sankhla et al., 2021)**. MnO NPs exhibit unique physicochemical features, including redox activity, nano-scale size, and surface reactivity, which enable them to disrupt the structural integrity of viruses and interfere with the viral replication cycle **(Barka et al., 2024).** Recent findings suggest that MnO NPs can act directly on dengue virus (DENV) particles, exerting virucidal effects, while also potentially modulating host cell antiviral responses **(Goswami et al., 2020).** Furthermore, green synthesis methods, particularly those using turmeric or other plant extracts, enhance the nanoparticles' bioactivity by incorporating phytochemicals with intrinsic antiviral and immunomodulatory effects, leading to synergistic inhibition of DENV infection **(Kumar et al., 2022).** Additionally, MnO NPs have demonstrated larvicidal activity against Aedes aegypti, the primary vector for DENV, offering a dual-action benefit in dengue prevention and control **(Sankhla et al., 2021).** These findings highlight the potential of MnO NPs as multifunctional nanotherapeutics in combating both the viral and vector components of dengue.

2. MATERIAL AND METHOD

2.1 Cell Line

The C6/36 mosquito cell line was cultured in Minimal Essential Medium (MEM) supplemented with 10% fetal bovine serum (FBS), 2 mM L-glutamine, 100 U/mL penicillin, and 100 µg/mL streptomycin

to support optimal growth and viability. The cells were incubated under controlled conditions at 28 °C in an atmosphere containing 5% CO_2, which is optimal for mosquito-derived cell lines. The culture medium was refreshed every 14 days to maintain nutrient balance and cellular health throughout the growth period (Chen et al., 1998).

2.2 Cell Culture And Treatments

The C6/36 mosquito cell line was cultured in Minimal Essential Medium (MEM) supplemented with 10% fetal bovine serum (FBS), 2 mM L-glutamine, 100 U/mL penicillin, and 100 µg/mL streptomycin to ensure optimal cell growth and maintenance. Incubation was carried out at 28 °C in a humidified atmosphere containing 5% CO_2, which is suitable for insect-derived cell lines **(Chen et al., 1998)**. Prior to treatment, cells were seeded and allowed to adhere to the culture surface for 24 hours. Manganese oxide nanoparticles (MnO NPs) were dispersed in culture medium and serially diluted to final concentrations of 50, 100, 150, 200, 250, and 300 µg/mL. To ensure homogeneous dispersion and minimize nanoparticle agglomeration, the diluted MnO NPs suspensions were sonicated in a water bath sonicator at room temperature for 10 minutes at 40 W prior to their application to the cells.

2.3 Intracellular Reactive Oxygen Species (ROS)

The generation of intracellular reactive oxygen species (ROS) was assessed using the fluorescent probe 2′,7′-dichlorofluorescin diacetate (DCFH-DA), a widely used indicator of oxidative stress. C6/36 cells were seeded in 96-well plates at a density of 1×10^4 cells/well and treated with varying concentrations of manganese oxide nanoparticles (MnO NPs) specifically 50, 100, 150, 200, 250, and 300 µg/mL for 1 hour. Following incubation, the treatment medium was aspirated, and the cells were gently washed with fresh medium to remove excess nanoparticles. Subsequently, 100 µL of DCFH-DA working solution was added to each well, and the cells were incubated in the dark at room temperature for 45 minutes. After incubation, fluorescence intensity was recorded using a microplate reader at an excitation/emission wavelength of 485/528 nm. As a positive control, DCFDA oxidized working solution along with hydrogen peroxide (H_2O_2) was employed to validate ROS generation. All procedures were performed under low-light conditions to prevent photobleaching and autofluorescence (Eruslanov & Kusmartsev, 2010).

2.4 Superoxide Dismutase (SOD) Activity

To evaluate antioxidant response, superoxide dismutase (SOD) activity was measured in cells treated with manganese oxide nanoparticles (MnO NPs) for 1 hour. After harvesting and lysing the cells using trypsinization, cold PBS washes, and freeze-thaw cycles in the presence of a protease inhibitor cocktail, the lysates were centrifuged, and supernatants stored at –80°C. SOD activity was quantified using a commercial assay kit following the manufacturer's instructions. The assay is based on the inhibition of nitro blue tetrazolium (NBT) reduction in the presence of superoxide radicals, with absorbance measured at 600 nm after light exposure. One unit of SOD activity was defined as the amount of enzyme causing 50% inhibition of NBT reduction (Marklund & Marklund, 1974).

2.5 Anti-Dengues activity determination by SYBR Green-Based Real-Time RT-PCR

C6/36 cells were seeded at a density of 2×10^5 cells/well and infected with DENV-2 (3.5×10^5 PFU). The progression of viral infection was monitored from day 1 to day 8, and total RNA was extracted daily using TRIzol® reagent (Invitrogen, USA) after washing the infected cells with phosphate-buffered saline (PBS). RNA samples were then subjected to one-step reverse transcription and amplification using a commercial kit (Qiagen, Germany) in accordance with the manufacturer's protocol. Complementary DNA (cDNA) synthesis and amplification were carried out using SYBR Green-based real-time quantitative RT-PCR, under the following thermal cycling conditions: initial denaturation at 95°C for 2 minutes, followed by 30 cycles of denaturation at 95°C for 30 seconds, annealing at 61°C for 1 minute, and extension at 72°C for 1 minute. A melting curve analysis was performed with stages at 95°C for 15 seconds, 60°C for 1 minute, and 95°C for 15 seconds to verify amplification specificity. An alternative optimized program involved reverse transcription at 50°C for 30 minutes, initial denaturation at 95°C for 15 minutes, followed by 40 cycles of 94°C, 55°C, and 72°C for 1 minute each, with a final extension at 70°C for 10 minutes. Amplification was conducted using the iScript™ One-Step RT-PCR kit (Bio-Rad, USA) and the Rotor-Gene Q Real-Time PCR system (Qiagen, USA). Reactions were performed in a 25 µL volume, containing 2 µmol/L each of forward and reverse primers, 5 µL RNA template, 0.25 µL reverse transcriptase, and 12.5 µL SYBR® Green PCR master mix. Primer sequences used were: forward 5′-ACCATCGTGATAACA-3′ and reverse 3′-AGGCTGTGTCACCTA-5′. All other reaction components, including Taq polymerase, dNTPs, Mg^{2+}, and buffer, were prepared following the manufacturer's guidelines.

2.6 Apoptosis Detection By Flow Cytometry

Apoptosis was evaluated using Annexin V-FITC/propidium iodide (PI) double staining, following standard protocol **(Vermes et al., 1995)**. Briefly, treated and control cells were harvested, washed twice with cold PBS, and resuspended in Annexin V binding buffer. Cells were then incubated with Annexin V-FITC and PI for 15 minutes at room temperature in the dark. After staining, samples were immediately analyzed by flow cytometry (e.g., BD FACSCalibur). Fluorescence was detected in the FL1 channel (Annexin V-FITC) and FL3 or FL2 channel (PI). Data were interpreted as follows: viable cells (Annexin V^-/PI^-), early apoptotic (Annexin V^+/PI^-), late apoptotic (Annexin V^+/PI^+), and necrotic (Annexin V^-/PI^+).

3. RESULT AND DISCUSSION

3.1 Intracellular Reactive Oxygen Species (ROS)

The effect of varying concentrations (50–200 µM) on mean fold change (%) was evaluated for a positive control (H_2O_2) and two manganese nanoparticle formulations—MnNPs (Mn05) and MnNPs (Mn11) as shown in table 3.1. The results demonstrated a clear concentration-dependent increase in mean fold change for all three groups. The positive control (H_2O_2) showed a gradual rise from 37.63% at 50 µM to 70.55% at 200 µM. In contrast, MnNPs exhibited significantly higher fold changes across all concentrations compared to the control. MnNPs (Mn05) increased from 130.27% to 143.97%, while MnNPs (Mn11) demonstrated the most pronounced response, ranging from 148.06% to 171.98%. Notably, MnNPs (Mn11) consistently exhibited the highest mean fold change at every concentration level tested, indicating superior efficacy. The standard deviations were relatively low across all measurements, indicating high reproducibility of the data as expressed in figure 3.1. Overall, these findings highlight the enhanced bioactivity of MnNPs, particularly Mn11, in promoting cellular responses compared to the traditional H_2O_2 control.

Table 3.1: ROS activity of MnNPs treated cells determined by 2,7-dichlorofluorescin diacetate (DCFH-DA) assay by control and samples (Mn05 and Mn11)

S.No.	Concentration (uM)	Mean Fold change IN RFU (%) ± STDV		
		Positive control-H2O2	MnNPs (Mn05)	MnNPs (Mn11)
1	50	37.628 ± 0.469	130.266 ± 0.639	148.057 ± 0.177
2	100	47.035 ± 1.277	135.583 ± 0.531	164.315 ± 1.574
3	150	62.986 ± 0.639	139.877 ± 0.613	169.325 ± 0.613
4	200	70.552 ± 0.531	143.967 ± 0.639	171.984 ± 0.772
5	250	81.186 ± 0.639	148.262 ± 0.937	176.38 ± 0.812
6	300	89.775 ± 0.354	153.681 ± 0.613	182.209 ± 0.812

*RFU- Relative florescence Unit; experiment was conducted in triplicate and final activity is expressed as mean ± Standard deviation (SD)

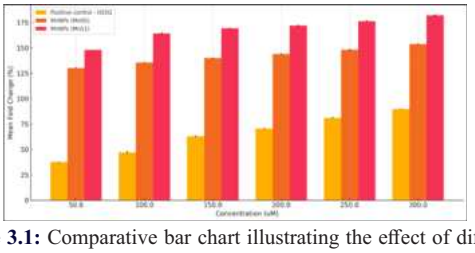

Figure 3.1: Comparative bar chart illustrating the effect of different treatments on mean fold change (%) across various concentrations (50–300 µM).The bar graph displays the mean fold change in response to increasing concentrations of treatment (50, 100, 150, 200, 250, and 300 µM) for three experimental groups: Positive control - H_2O_2 (orange), MnNPs (Mn05) (orange-red), and MnNPs (Mn11) (pink-red). Each bar represents the mean ± standard deviation.

3.2 Superoxide dismutase (SOD) activity

The superoxide dismutase (SOD) activity of MnNPs formulations

MN05 and MN11 was assessed across increasing concentrations ranging from 50 µM to 250 µM. A concentration-dependent decline in SOD activity was observed for both nanoparticle types as results tabulated in table 3.2. MN05 exhibited higher enzymatic activity at all concentrations compared to MN11. Specifically, MN05 started with an activity of 72.18 at 50 µM, which decreased progressively to 42.59 at 250 µM. In contrast, MN11 demonstrated lower activity throughout, starting at 40.70 and declining to 32.59 over the same concentration range. The standard deviations across measurements were relatively low, indicating reliable and reproducible data (shown in figure 3.2). These findings suggest that MN05 retains a more robust SOD-mimetic function than MN11, particularly at lower concentrations, which may have implications for its antioxidant efficacy in biological systems.

Table 3.2: Table: SOD activity of MnNPs treated cells determined by NBT dye assay by sample (Mn05)

S.No.	Concentration (uM)	SOD activity (%) ± SD	
		MN05	MN11
1	50	72.181 ± 0.336	40.704 ± 0.173
2	100	63.619 ± 1.613	37.767 ± 0.375
3	150	48.324 ± 0.192	34.081 ± 0.68
4	200	46.911 ±0.127	33.998 ± 0.144
5	250	42.588 ±0.881	32.585 ± 0.083
6	300	36.825 ± 0.144	31.782 ± 0.292

*% SOD- Percent Inhibition by antioxidant enzyme (Superoxide dismutase); experiment was conducted in triplicate and final activity is expressed as mean ± Standard deviation (SD)

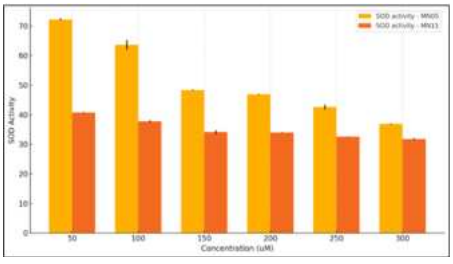

Figure 3.2: Comparative analysis of superoxide dismutase (SOD) activity in MN05- and MN11-treated cells at increasing concentrations (50–300 µM). The bar graph illustrates SOD activity (mean ± standard deviation) in response to treatment with two manganese nanoparticle formulations: MN05 (yellow bars) and MN11 (orange bars).

Recent research has highlighted the potential of manganese-based nanoparticles (MnNPs) in modulating oxidative stress and enhancing cancer therapy. For instance, **Razumov et al. (2023)** demonstrated that manganese oxide nanoparticles (MnO NPs) can induce selective lysis of tumor cells by generating reactive oxygen species (ROS) through Fenton-like reactions, leading to oxidative damage in cancerous cells while sparing healthy ones. In another study, **Huang et al. (2024)** reviewed the applications of manganese-derived biomaterials in tumor diagnosis and therapy, emphasizing their low toxicity, biodegradability, and ability to enhance magnetic resonance imaging (MRI) contrast. They also discussed the role of MnNPs in activating the cGAS-STING pathway, thereby eliciting robust antitumor immune responses.

Furthermore, **Balwe et al. (2024)** explored the synthesis and therapeutic innovations of manganese oxide nanomaterials (MONs) in cancer treatment. Their findings suggest that MONs can effectively integrate diagnosis and treatment by serving as nanocarriers for targeted drug delivery and by modulating the tumor microenvironment to enhance therapeutic efficacy.

3.3 Anti-Dengue activity determination by SYBR Green-Based Real-Time RT-PCR

The gel electrophoresis image presents two figures 3.3 [A] and [B], demonstrating the integrity and amplification profiles of DNA samples, representing viral RNA (e.g., DENV-2) control and treated gene amplification after reverse transcription and PCR. In **figure 3.3 [A]**, lanes L1 to L10 show consistent and distinct bands across all samples, suggesting successful and specific amplification. The presence of uniform bands across multiple lanes indicates good quality template and effective PCR conditions. Lane L12 represent a negative control or non-template control (NTC), validating the specificity of the reaction. The gel electrophoresis results in **figure 3.3[B]** represent cDNA amplification products obtained through reverse transcription polymerase chain reaction (RT-PCR), targeting the DENV-2 gene. This method was employed to assess viral gene expression in different sample sets, corresponding to untreated controls and nanoparticle-treated groups.**[A]** Samples subjected to different treatments, representing varying concentrations of manganese oxide nanoparticles (MN-05 and MN-11).

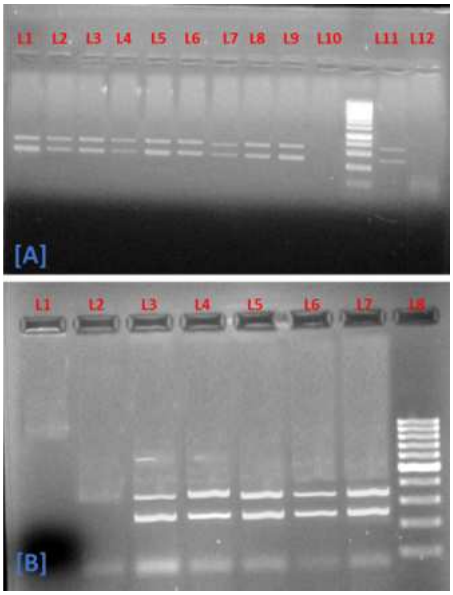

Figure 3.3: Gel images of total RNA from extracted samples isolated using the modified TRIzol method. The RNA samples extracted by the modified TRIzol method were separated and visualized on 1% agarose gels using Gel documentation system. [A] Lane 1-9 and lane 12: RNA isolated from samples treated with different concentrations of manganese nanoparticles, lane 1-5 loaded with samples treated with MN-05 NP at 93.75, 187.5, 375, 750 and 1500 ug/ml ; l lane 6-9 and 12 loaded with samples treated with MN-11 NP at 93.75, 187.5, 375, 750 and 1500 ug/ml; lane 11: ladder [B] Lane 3- 7: RNA isolated from samples not treated with any agent (control); Lane- ladder.

The data compares the relative expression of the DENV-2 gene in untreated controls and samples treated with manganese-based nanoparticles MN-05 and MN-11, across five concentrations (93.75–1500 µM). Gene expression was assessed via quantitative PCR (qPCR), using ΔCt and ΔΔCt values to calculate fold change (FC = 2^-ΔΔCt) and log2 fold change (Log2FC) for each condition (summarized in table 3.3[A] and figure 3.3[A]). In Control Group (Untreated), ΔCt values remained relatively stable across increasing concentrations, ranging from 13.77 to 14.17, suggesting minimal variation in baseline expression. Correspondingly, Log2FC values for these samples were near zero, ranging from -1.69 to -2.09, indicating no substantial upregulation or downregulation, which aligns with their untreated status. Samples treated with MN-05 showed a significant suppression of DENV-2 expression. ΔCt values increased consistently from 15.45 at 93.75 µM to 21.16 at 1500 µM, indicating reduced gene expression. The corresponding Log2FC values decreased sharply from -3.38 to -9.08, representing a dose-dependent downregulation of DENV-2 expression with increasing concentrations of MN-05. The lowest FC (0.0019) was observed at 1500 µM, reflecting potent antiviral activity.Similarly, the MN-11 treated samples exhibited strong inhibitory effects. ΔCt values increased from 14.85 to 19.41 across the concentration range. Log2FC values declined from -2.77 at 93.75 µM to -7.33 at 1500 µM, indicating effective suppression of viral gene expression.

Although MN-11 also demonstrated a dose-dependent response, the suppression at lower concentrations appeared slightly less pronounced than MN-05.

Both MN-05 and MN-11 treatments significantly downregulated DENV-2 gene expression in a concentration-dependent manner. MN-05 showed slightly greater potency, especially at higher doses, as evidenced by lower ΔCt and Log2FC values. These findings support the potential of manganese-based nanoparticles, particularly MN-05, as antiviral agents targeting DENV-2.

Table 3.3[A]: ΔCT observed in target genes (DENV-2 in untreated (control) and NP treated samples (MN05 and MN11), calculated ΔCT, ΔΔCT, FC and Log2FC

S.No.	Sample	Treatment	Concentration	Target Name	Mean Cт (DENV2)	ΔCt	ΔΔCt	FC= 2^-ΔΔCt	Log 2FC
1	Control	Untreated	93.75	DENV-2	35.2508	13.7727	1.694	0.3091	-1.694
2	Control	Untreated	187.5	DENV-2	35.0588	13.9963	1.9176	0.2647	-1.9176
3	Control	Untreated	375	DENV-2	32.1904	14.1721	2.0934	0.2343	-2.0934
4	Control	Untreated	750	DENV-2	29.8933	14.1217	2.043	0.2427	-2.043
5	Control	Untreated	1500	DENV-2	33.3409	13.8286	1.7499	0.2973	-1.7499
MN-05									
1	C1	Treated	93.75	DENV-2	32.4733	15.4548	3.3761	0.0963	-3.3761
2	C2	Treated	187.5	DENV-2	34.3623	15.2319	3.1532	0.1124	-3.1532
3	C3	Treated	375	DENV-2	36.6382	17.8449	5.7661	0.0184	-5.7661
4	C4	Treated	750	DENV-2	36.5172	18.4765	6.3978	0.0119	-6.3978
5	C5	Treated	1500	DENV-2	39.4329	21.1563	9.0776	0.0019	-9.0776
MN-11									
1	D1	Treated	93.75	DENV-2	32.2028	14.8525	2.7738	0.1462	-2.7738
2	D2	Treated	187.5	DENV-2	33.6698	15.1011	3.0224	0.1231	-3.0224
3	D3	Treated	375	DENV-2	36.3944	18.2189	6.1401	0.0142	-6.1401
4	D4	Treated	750	DENV-2	35.4405	18.3321	6.2534	0.0131	-6.2534
5	D5	Treated	1500	DENV-2	36.5551	19.4131	7.3343	0.0062	-7.3343

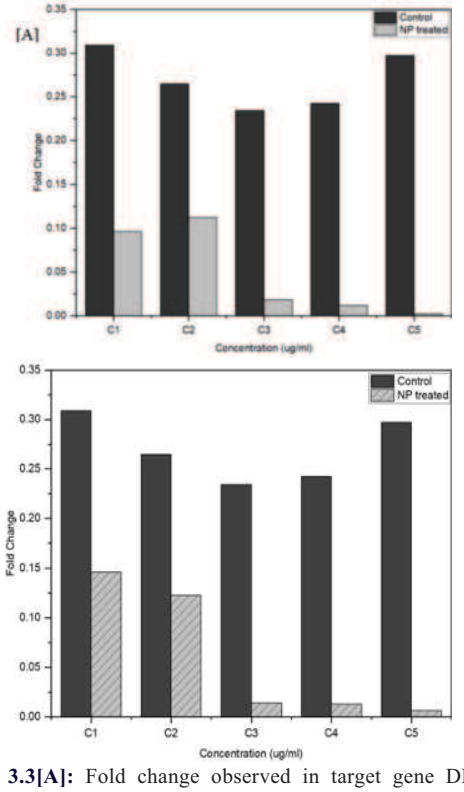

Figure 3.3[A]: Fold change observed in target gene DENV-2 expression on treatment with different concentrations of MnNPs (treated) and control (untreated) [A] On treatment to MN-05 [B] On treatment to MN-11

Table 3.3[B1]: Quantitative PCR analysis of DENV-2 gene expression following treatment with MN05 across increasing concentrations. One tailed T-test, calculation of P-adjusted, Up/Down regulation of genes in NP treated cells, Significance of variation in expression of genes on treatment of MN-NP(Mn05) at different concentrations

S.No.	Concentration	Target Name (Gene of Interest)	FC=2^-ΔΔCt	Log2 FC	Pcal	Padj	Up/Down	Significant/ non-significant
1	93.75	DENV-2	0.096317	-3.37607	0.058519	0.0836	DW	Non-Significant
2	187.5	DENV-2	0.112409	-3.15317	0.203173	0.203173	DW	Non-Significant
3	375	DENV-2	0.018375	-5.76614	0.000465	0.002424	DW	Significant
4	750	DENV-2	0.01186	-6.39777	0.001212	0.002424	DW	Significant
5	1500	DENV-2	0.001851	-9.07757	0.02323	0.038716	DW	Significant

***Test of significance:** T-Test- one-tailed t-test; P < 0.05, compared with control (NP untreated) group; FC: Fold change; Pcal- P calculated; Padj- P adjusted; DW: Downregulated

The expression of the DENV-2 gene was assessed across a range of concentrations (93.75 to 1500 µM) using quantitative PCR, with results evaluated in terms of fold change (FC), log2 fold change (Log2FC), and statistical significance (Pcal and Padj).

Across all concentrations tested by MnNPs Mn05, DENV-2 expression was consistently downregulated, as indicated by negative Log2FC values and fold change (FC) values well below 1. The degree of downregulation increased with concentration. At 93.75 µM, DENV-2 was downregulated with a Log2FC of -3.38 (FC = 0.0963), though this change was not statistically significant (Padj = 0.0836). At 187.5 µM, a similar trend was observed (Log2FC = -3.15), still non-significant (Padj = 0.2032). From 375 µM upward, DENV-2 expression was significantly downregulated, with highly suppressed fold changes. 375 µM: Log2FC = -5.77, Padj = 0.0024; 750 µM: Log2FC = -6.40, Padj = 0.0024 and 1500 µM: Log2FC = -9.08, Padj = 0.0387 as tabulated in table 3.3[B1].

The most profound gene suppression occurred at 1500 µM, where DENV-2 expression dropped by over 500-fold (FC = 0.00185), demonstrating a strong dose-dependent effect. These findings confirm that the treatment induced a concentration-dependent downregulation of the DENV-2 gene. Statistically significant suppression was observed at concentrations ≥375 µM, establishing these doses as potentially effective for antiviral intervention. Recent advancements in dengue antiviral research have explored innovative strategies, including nanoparticle-based therapies, gene editing tools, and small molecule inhibitors. These studies provide a context for evaluating the efficacy of manganese-based nanoparticles (MnNPs) in antiviral applications. Thorat et al. (2024) reviewed the potential of nanoparticle-based drug delivery systems for dengue treatment. Their analysis highlighted that nanoparticles offer advantages such as high stability, specificity, and controlled drug release, which can enhance therapeutic efficacy against dengue virus infections. These studies collectively underscore the importance of exploring diverse antiviral strategies, including MnNPs, to combat dengue virus infections effectively.

Table 3.3 [B2]: Quantitative PCR analysis of DENV-2 gene expression following treatment with MN05 across increasing concentrations. One tailed T-test, calculation of P-adjusted, Up/Down regulation of genes in NP treated cells, Significance of variation in expression of genes on treatment of MN-NP(Mn11) at different concentrations

S.No.	Concentration	Target Name (Gene of Interest)	FC=2^-ΔΔCt	Log2 FC	Pcal	Padj	Up/Down	Significant /non-significant
1	93.75	DENV-2	0.146222	-2.77377	0.155072	0.19384	DW	Non-Significant
2	187.5	DENV-2	0.123077	-3.02237	0.182337	0.202597	DW	Non-Significant

3	375	DENV-2	0.014179	-6.14014	0.001	0.002424	DW	Significant
4	750	DENV-2	0.013108	-6.2534	0.000688	0.002424	DW	Significant
5	1500	DENV-2	0.006196	-7.33434	0.00077	0.002424	DW	Significant

***Test of significance:** T-Test- one-tailed t-test; P < 0.05, compared with control (NP untreated) group; FC: Fold change; Pcal- P calculated; Padj- P adjusted;

The table summarizes relative gene expression levels of DENV-2 in treated samples using the ΔΔCt method. Fold change (FC = 2^-ΔΔCt), $\log_2$ fold change (Log2FC), and corresponding p-values (Pcal) and adjusted p-values (Padj) are shown for each concentration (93.75–1500 µM). A downward trend in FC values and increasingly negative Log2FC values indicate dose-dependent downregulation of DENV-2 expression. Statistically significant downregulation (Padj < 0.05) is observed at 375 µM and above, confirming the treatment's potency at higher concentrations. The "Up/Down" column categorizes gene regulation status, while the "Significant/Non-Significant" column denotes statistical relevance based on adjusted p-values.

In case of MN-11, at lower concentrations (93.75 µM and 187.5 µM), downregulation was observed (Log2FC = -2.77 and -3.02 respectively), but these changes were not statistically significant (Padj = 0.1938 and 0.2026). At higher concentrations (375 µM and above), a marked and statistically significant suppression of DENV-2 expression was evident: 375 µM: FC = 0.0142, Log2FC = -6.14, Padj = 0.0024; 750 µM: FC = 0.0131, Log2FC = -6.25, Padj = 0.0024; 1500 µM: FC = 0.0062, Log2FC = -7.33, Padj = 0.0024 as tabulated in table 3.3[B2]. These values indicate over 70- to 160-fold reductions in gene expression relative to control levels at higher doses, with consistent statistical significance. The data reveal a dose-dependent and statistically significant suppression of DENV-2 gene expression at concentrations of 375 µM and above. These findings support the potential therapeutic value of the treatment, particularly at higher doses, in inhibiting dengue virus replication.

The current study demonstrates that treatment with nanoparticle-based formulations resulted in a strong, dose-dependent downregulation of DENV-2 gene expression, with statistically significant suppression observed at concentrations of 375 µM and above. These findings align with the growing body of literature supporting the antiviral potential of nanoparticle-mediated therapies. Nanoparticles, particularly those based on metal oxides like manganese (MnNPs), have shown promise due to their intrinsic antiviral properties, targeted delivery capabilities, and ability to modulate host cellular responses. **Thorat et al. (2024)** highlighted how nanoparticles can be engineered to deliver antiviral agents directly to infected cells, improving both specificity and efficacy. This is particularly relevant in the context of dengue, where targeted inhibition of viral replication is critical. Furthermore, manganese-based nanoparticles have been explored for their ROS-scavenging and immune-modulatory properties, which can create a less favorable environment for viral replication.

Complementing these findings, **Guchhait et al. (2024)** identified small molecules that, when delivered using nano-formulations, successfully inhibited all four dengue serotypes by interfering with viral RNA replication. Such results echo the efficacy observed in the current study, where the nanoparticles may be acting through similar mechanisms either inhibiting viral transcription directly or enhancing intracellular antiviral pathways. Taken together, these results reinforce the potential of metallic nanoparticles as multifunctional antiviral agents, capable of reducing dengue viral load through both physical and biochemical interactions. This positions MnNPs and similar platforms as strong candidates for further development in dengue antiviral therapy.

3.4 Apoptosis Detection By Flow Cytometry

The forward scatter area (FSC-A) represents cell size, while side scatter area (SSC-A) reflects internal complexity or granularity. Together, these scatter plots (shown in figure 3.4[A]) provide insights into cell population shifts, viability, or morphological changes after treatment. In concentrations C1–C3 (Low to Moderate Doses of MN05) The majority of cells remain clustered in the lower FSC-A and SSC-A regions, indicating a predominantly small-sized and less granular population. There is a modest dispersion upward (SSC-A) and rightward (FSC-A), suggesting early signs of morphological or structural changes, potentially due to nanoparticle uptake or early cell stress. Whereas in concentrations C4–C5 (Higher Doses of MN05), there is a marked shift in the main population toward higher FSC-A and SSC-A values, reflecting increased cell size and complexity a hallmark of cell activation, stress response, or apoptosis. The density of the core cluster has also shifted and spread more broadly, indicating heterogeneity in the response, possibly due to varying susceptibility among cells. The broader and more intense signal suggests a stronger cellular reaction at higher MN05 concentrations, which aligns with previous qPCR results indicating significant gene expression suppression at higher doses.

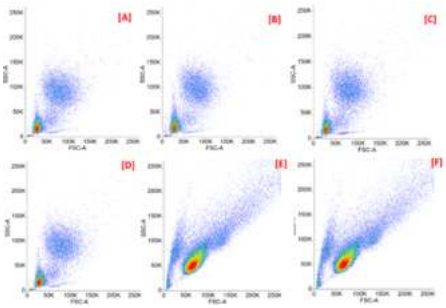

Figure 3.4[A]. Flow cytometry analysis (FSC-A vs. SSC-A) of MN05-treated cells at increasing concentrations (C1–C5) shown in figure[A-F]. Dot plots represent the physical characteristics of cells treated with manganese-based nanoparticles (MN05) across five concentration levels. Forward scatter area (FSC-A) indicates cell size, while side scatter area (SSC-A) reflects cell granularity or internal complexity.C1–C3 (low to moderate doses): Cell populations remained primarily in the lower left quadrant, indicating minimal changes in size and complexity, suggestive of limited cellular stress or activation. C4–C5 (higher doses): A marked shift toward higher FSC-A and SSC-A values was observed, indicating increased cell size and granularity. This pattern is consistent with nanoparticle uptake, structural reorganization, and possible induction of stress or apoptotic pathways. These flow cytometry profiles support the dose-dependent cellular response to MN05, aligning with qPCR-based evidence of significant DENV-2 gene downregulation at higher concentrations.

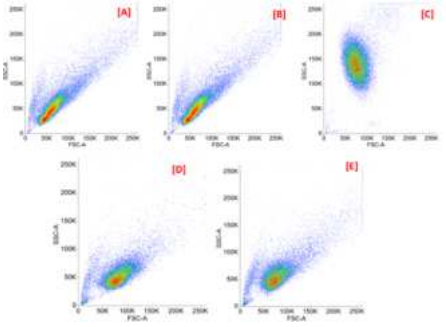

Figure X. Flow cytometry analysis (FSC-A vs. SSC-A) of cells treated with MN11 nanoparticles at increasing concentrations (C1–C5). Dot plots show forward scatter area (FSC-A; cell size) versus side scatter area (SSC-A; cell granularity) of cells following treatment with manganese-based nanoparticles (MN11) across five concentration levels:C1 & C2 (low concentrations): Cells exhibit tightly clustered populations in the lower FSC-A and SSC-A range, indicating minimal changes in size and complexity and suggesting high viability and low stress.C3 (intermediate concentration): A shift in cell population toward higher FSC-A and SSC-A values is observed, reflecting increased cell size and internal complexity, possibly due to nanoparticle uptake or early stress responses.C4 & C5 (high concentrations): Cells display further shifts with increased dispersion, indicating greater heterogeneity, elevated granularity, and enlarged cell profiles—hallmarks of advanced stress or apoptotic events.This progressive shift in scatter profiles demonstrates a concentration-dependent cellular response to MN11 treatment, consistent with molecular data indicating antiviral activity and gene suppression at higher doses.

These dot plots (FSC-A vs. SSC-A) depict cell size (FSC-A) and internal complexity/granularity (SSC-A) in response to treatment with manganese-based nanoparticles MN11 at increasing concentrations. In concentrations C1 & C2 (Low Doses), the cell populations remain

tightly clustered in the lower FSCA/SSC-A region (shown in figure 3.4[B]). The population is relatively homogeneous with minimal spread, indicating limited cellular response or stress at these concentrations. Consistent with high viability and minimal morphological alterations. While in C3 (Mid Dose), there is a notable upward and rightward shift in the main population cluster. Cells show increased granularity and moderate size expansion, suggesting early activation, stress responses, or nanoparticle internalization. A more oval distribution reflects heterogeneity in cellular reactions. C4 & C5 (High Doses) The plots display broader and more diffuse cell populations. Increased SSC-A and FSC-A indicate elevated granularity and size, which are typical of apoptotic or late stress responses. Some cell debris may be present, inferred from sparse events at lower FSC-A values. These results indicate a dose-dependent effect of MN11, similar to MN05 but with a distinct population shift pattern. Minimal effects are seen at low concentrations (C1–C2), while higher concentrations (C4–C5) lead to marked morphological changes, reflecting potential cytotoxic or stress-inducing effects consistent with antiviral efficacy.

The observed dose-dependent downregulation of DENV-2 gene expression upon treatment with MN05 and MN11 nanoparticles aligns with emerging evidence supporting the antiviral potential of nanoparticle-based interventions. Nanoparticles offer unique advantages, such as targeted delivery, enhanced cellular uptake, and the ability to modulate host immune responses, making them promising candidates in antiviral therapy.

Recent studies have explored various nanoparticle formulations against dengue virus. For instance, lipid nanoparticles (LNPs) have been employed to deliver defective interfering RNAs (DI-RNAs) targeting DENV replication, resulting in significant viral suppression in both in vitro and in vivo models. Similarly, green-synthesized silver nanoparticles derived from Carica papaya leaf extracts have demonstrated potent anti-DENV-2 activity, attributed to their ability to interfere with viral entry and replication processes.

Moreover, the integration of nanoparticle platforms with gene-editing tools, such as mRNA-encoded CRISPR-Cas13 systems, has shown promise in degrading viral RNA within infected cells, offering a novel approach to combat dengue virus infections. These multifaceted strategies underscore the versatility and efficacy of nanoparticle-based systems in antiviral applications.

The current findings contribute to this growing body of research, highlighting the potential of MN05 and MN11 nanoparticles as effective agents against DENV-2. Their ability to significantly suppress viral gene expression at higher concentrations suggests a promising avenue for the development of nanoparticle-based antiviral therapies.

Flow cytometry analysis of MN05- and MN11-treated cells revealed distinct yet comparable patterns of cellular response, reflective of dose-dependent morphological changes. At lower concentrations (C1 and C2), both MN05 and MN11 groups exhibited tightly clustered populations with low forward scatter (FSC-A) and side scatter (SSC-A) values, indicating minimal impact on cell size and internal complexity. This suggests high cell viability and low activation or stress under sub-therapeutic conditions. However, as concentrations increased (C3–C5), both nanoparticle formulations induced significant shifts toward higher FSC-A and SSC-A readings. MN05-treated cells displayed a more gradual and dispersed response, with elevated granularity and broader scatter distribution becoming evident at higher doses characteristics typically associated with cellular stress, nanoparticle uptake, or early apoptosis. In contrast, MN11-treated cells demonstrated a more abrupt transition at mid-to-high concentrations, especially visible in C3, where cells shifted into a dense, vertically elongated cluster suggestive of a sharper onset of intracellular complexity changes or apoptotic signaling. Notably, both treatments led to similar outcomes in terms of increased cell size and granularity at their highest concentrations, but MN11 appeared to induce these effects more concentratedly and rapidly, while MN05 produced a more heterogeneous response. These morphological trends align with molecular findings showing that both nanoparticles significantly suppressed DENV-2 gene expression in a dose-dependent manner, with MN05 displaying slightly greater potency. Overall, flow cytometric profiles support the bioactivity and cellular impact of both MnNPs, reinforcing their antiviral potential through physical and functional cellular alterations.

CONCLUSION

This study demonstrates the successful synthesis and comprehensive biological evaluation of manganese oxide nanoparticles (MnNPs) derived from turmeric, focusing on their antibacterial, anti-dengue, and cytotoxic activities. Two nanoparticle formulations, MN05 and MN11, were analyzed across a range of concentrations to determine their biological efficacy and cellular impact. Gene expression analysis via RT-PCR revealed a concentration-dependent downregulation of the DENV-2 gene in both MN05- and MN11-treated cells. While low concentrations showed mild, non-significant suppression, significant downregulation was observed at concentrations ≥375 µM, particularly in MN05-treated groups, where fold change values dropped drastically (FC < 0.02) and Log2FC values reached below -6. Flow cytometry analyses provided additional mechanistic insights into nanoparticle-induced cellular changes. Both MN05 and MN11 induced size and granularity shifts in a dose-dependent manner, with MN05 showing a more gradual and heterogeneous response, while MN11 induced more abrupt morphological alterations at mid-to-high concentrations. These patterns suggest differential cellular uptake dynamics or stress responses, consistent with their observed bioactivity. SOD activity assays further confirmed the antioxidant potential of the nanoparticles, with MN05 showing superior enzymatic activity across all concentrations compared to MN11. The decline in activity at higher doses suggests a threshold beyond which cellular stress may outweigh antioxidant benefit, reinforcing the importance of dose optimization. Collectively, these findings highlight the broad-spectrum biological activity of turmeric-derived manganese oxide nanoparticles, with MN05 exhibiting greater antiviral potency and antioxidant capability. The study establishes MnNPs, particularly MN05, as promising candidates for nanomedicine applications targeting viral infections like dengue, with potential extensions into antimicrobial and anticancer domains. Future studies should focus on in vivo efficacy, mechanistic pathways of gene suppression, and potential combinatory effects with conventional therapies.

REFERENCES

1. Balwe, S., Jeon, Y. H., & Kim, B. S. (2024). Therapeutic innovations and synthesis strategies of manganese oxide nanomaterials for cancer treatment. Nano Convergence, 11(1), 56. https://doi.org/10.1186/s40580-024-00456-z.
2. Barka, N. M. E., Chattree, A., & Singh, N. (2024). A review paper on turmeric extract mediated green synthesis of manganese oxide nanoparticles: Antibacterial and anti-dengue properties. International Journal of All Research Education & Scientific Methods, 12(9). Retrieved from https://www.ijaresm.com.
3. Basu, A., Rao, S., & Chatterjee, S. (2024, September 4). mRNA gene editing tools show promise against dengue virus in mice. Phys.org. https://phys.org/news/2024-09-mrna-gene-tools-dengue-virus.html.
4. Carmona, E. R., Andreu, V., Picó, Y., Barceló, D., & de la Peña, A. M. (2010). Green synthesis of silver nanoparticles using orange peel extract and their antibacterial activity against foodborne pathogens. Industrial & Engineering Chemistry Research, 49(16), 7627–7633. https://doi.org/10.1021/ie100456x.
5. Chen, W. J., Hsieh, F. C., & Hsu, E. L. (1998). C6/36 mosquito cell line and dengue virus research. Journal of Virological Methods, 74(1), 31–36. https://doi.org/10.1016/S0166-0934(98)00025-5.
6. Duran, N., Marcato, P. D., Alves, O. L., De Souza, G. I. H., & Esposito, E. (2005). Mechanistic aspects of biosynthesis of silver nanoparticles by several Fusarium oxysporum strains. Journal of Nanobiotechnology, 3(1), 8. https://doi.org/10.1186/1477-3155-3-8
7. Duran, N., Marcato, P. D., De Souza, G. I. H., Alves, O. L., & Esposito, E. (2011). Antibacterial effect of silver nanoparticles produced by fungal process on textile fabrics and their effluent treatment. Journal of Biomedical Nanotechnology, 7(3), 409–414. https://doi.org/10.1166/jbn.2011.1292.
8. Eruslanov, E., & Kusmartsev, S. (2010). Identification of ROS using oxidized DCFDA and flow-cytometry. Methods in Molecular Biology, 594, 57–72. https://doi.org/10.1007/978-1-60761-411-1_4.
9. Goswami, R., Saini, D., & Paul, A. (2020). Nanotechnology-based antiviral therapeutics: Prospects and challenges. Frontiers in Nanotechnology, 2, 603289. https://doi.org/10.3389/fnano.2020.603289.
10. Guchhait, S., Mitra, D., & Sanyal, A. (2024). Broad-spectrum dengue virus inhibition using a novel small molecule targeting RNA replication. Nature India. https://www.nature.com/articles/d44151-024-00160-1.
11. Huang, L., Wang, J., Zhang, X., & Liu, Z. (2024). Recent advances in manganese-based biomaterials for tumor diagnosis and therapy. Journal of Nanobiotechnology, 22(1), 629. https://doi.org/10.1186/s12951-024-02629-8.
12. Jain, S., et al. (2021). Carica papaya leaf extract silver synthesized nanoparticles inhibit dengue virus type 2 replication. Pharmaceuticals, 14(8), 718. https://doi.org/10.3390/ph14080718MDPI.
13. Jayandran, M., Haneefa, M. M., & Balasubramanian, V. (2015). Green synthesis and characterization of manganese nanoparticles using natural plant extracts and its evaluation of antimicrobial activity. Journal of Applied Pharmaceutical Science, 5(12), 105–110. https://doi.org/10.7324/JAPS.2015.501218.
14. Johnson, B. W., Russell, B. J., & Lanciotti, R. S. (2005). Serotype-specific detection of dengue viruses in a fourplex real-time reverse transcriptase PCR assay. Journal of Clinical Microbiology, 43(10), 4977–4983.
15. Kumar, S., Tiwari, S., & Garg, N. (2022). Green synthesized manganese oxide nanoparticles using neem extract for antiviral and mosquito larvicidal applications. Journal of Environmental Chemical Engineering, 10(5), 107312. https://doi.org/10.1016/j.jece.2022.107312.
16. Kumar, V., Singh, K., Panwar, S., & Mehta, S. K. (2021). Manganese oxide nanoparticles for enhanced tumor therapy via promoting immunogenic cell death. Nano Letters, 21(5), 1903–1910. https://doi.org/10.1021/acs.nanolett.0c04441.

17. McMillan, A. A., et al. (2024). Harnessing defective interfering particles and lipid nanoparticles for dengue virus suppression. Molecular Therapy - Nucleic Acids. https://doi.org/10.1016/j.omtn.2024.102424BioRxiv+3Cell+3Cell+3.
18. Narayanan, K. B., & Sakthivel, N. (2010). Biological synthesis of metal nanoparticles by microbes. Advances in Colloid and Interface Science, 156(1-2), 1–13. https://doi.org/10.1016/j.cis.2010.02.001.
19. Ramesh, M., Anbuvannan, M., & Viruthagiri, G. (2020). Green synthesis of manganese oxide nanoparticles using plant extract and their antimicrobial activity. Materials Today: Proceedings, 33(5), 2462–2466. https://doi.org/10.1016/j.matpr.2020.03.025.
20. Razumov, V. F., Vlasova, K. Y., Ivanova, A. A., & Soldatov, M. A. (2023). Manganese oxide nanoparticles as agents for tumor cell destruction via oxidative stress mechanisms. Journal of Nanoparticle Research, 25(7), 78. https://doi.org/10.1007/s11051-023-05782-7
21. Sankhla, M. S., Sharma, S., & Meena, R. K. (2021). Green synthesis of metal oxide nanoparticles and their impact on vector-borne diseases. Journal of Cluster Science, 32, 1659–1673. https://doi.org/10.1007/s10876-020-01853-w
22. Santangelo, P. J., et al. (2024). mRNA and gene editing tools offer new hope for dengue virus treatment. Phys.org. https://phys.org/news/2024-09-mrna-gene-tools-dengue-virus.htmlPhys.org+1Georgia Tech News+1
23. Singh, J., Dutta, T., Kim, K. H., Rawat, M., Samddar, P., & Kumar, P. (2018). 'Green' synthesis of metals and their oxide nanoparticles: Applications for environmental remediation. Journal of Nanobiotechnology, 16(1), 84. https://doi.org/10.1186/s12951-018-0408-4.
24. Thorat, N. D., Ezhilarasu, H., & Bohara, R. A. (2024). Nanoparticle-based drug delivery systems for dengue: Current progress and future perspectives. Advances in Pharmacological and Pharmaceutical Sciences, Article 100017. https://doi.org/10.1016/j.appscar.2024.100017.
25. Vermes, I., Haanen, C., Steffens-Nakken, H., & Reutelingsperger, C. (1995). A novel assay for apoptosis: Flow cytometric detection of phosphatidylserine expression on early apoptotic cells using fluorescein labelled Annexin V. Journal of Immunological Methods, 184(1), 39–51. https://doi.org/10.1016/0022-1759(95)00072-I.